Rebound in epidemic control: How misaligned vaccination timing amplifies infection peaks

Supplementary Material

Piergiorgio Castioni, Sergio Gómez, Clara Granell, Alex Arenas

Departament d'Enginyeria Informàtica i Matemàtiques
Universitat Rovira i Virgili
43007 Tarragona, Spain

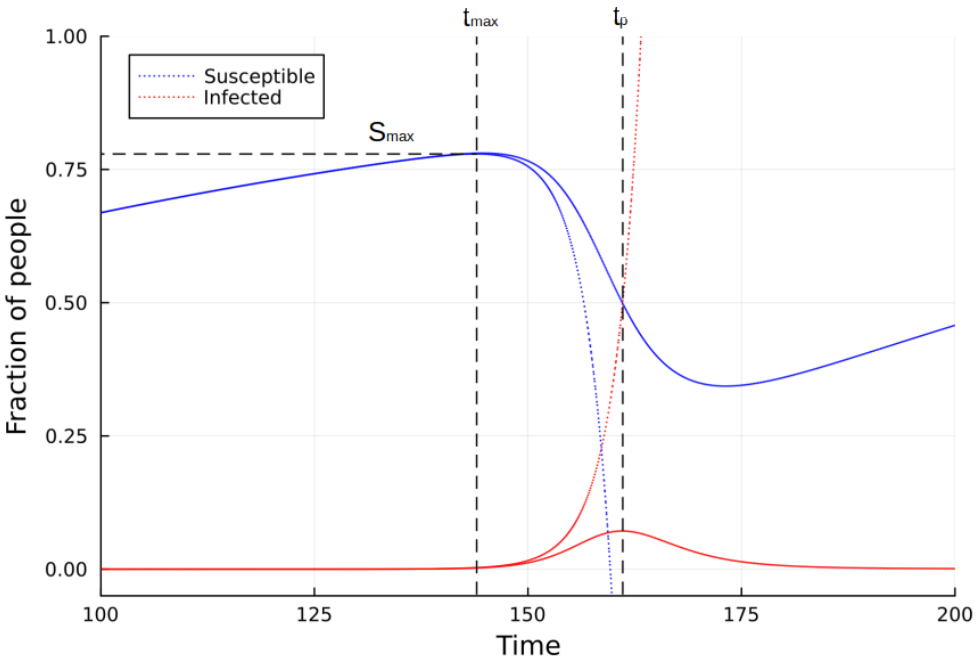

Fig. S1: **No-infected approximation of the SIRS model.** Comparison between the numerical solution of the SIRS model (solid lines) and the analytical formulas (dotted lines). The analytical formulas are the ones displayed in Eqs. (10)–(12) and obtained in the no-infected approximation. Here, only the susceptible and infected curves are shown. The two vertical lines correspond to $t_{\max}$ and t_p, which are the times at which the maximum of the susceptible curve $S_{\max}$ is reached and the estimated time of the peak, respectively. Simulation with $\beta = 1$, $\mu = 0.5$, $\delta = 0.01$, $S(0) = 0.1$, $I(0) = 10^{-4}$, here displayed only between the times $t = 100$ to $t = 200$.

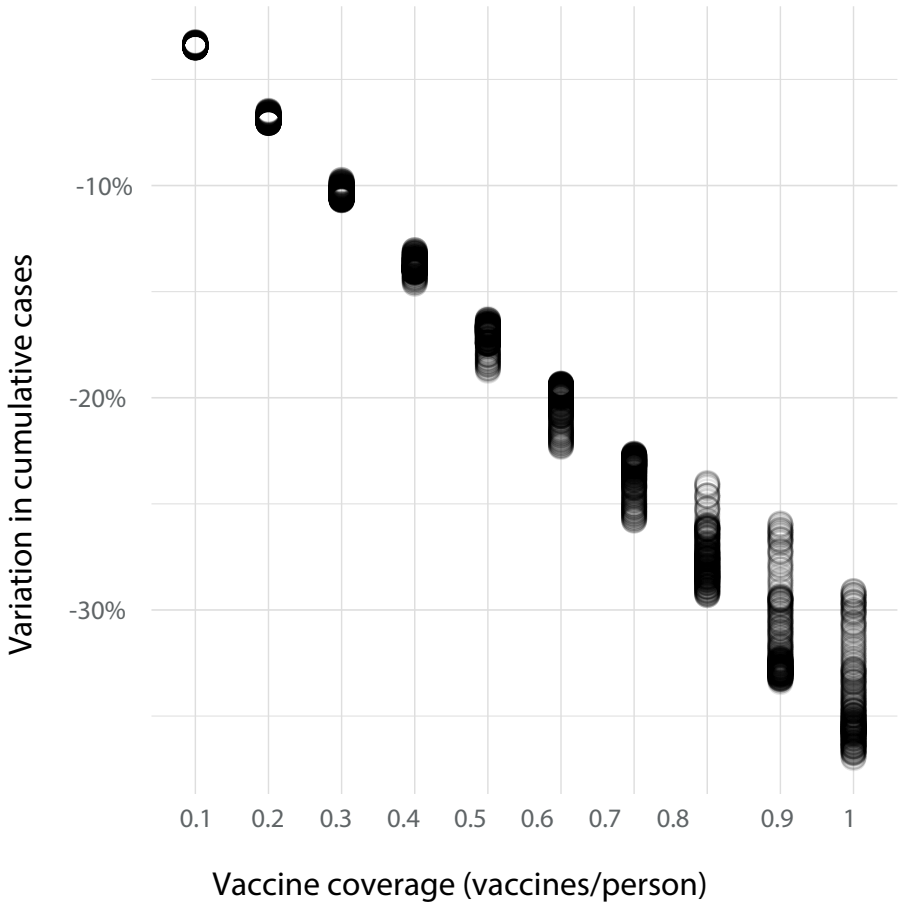

Fig. S2: **Relative reduction in cumulative cases.** Relative reduction in cumulative cases with respect to the scenario with no vaccines as a function of the vaccine coverage, defined as the ratio of vaccines with respect to the total population. Each circle in the figure denotes a specific simulation characterized by a constant vaccine coverage, starting time, and campaign duration. It is evident from the data that vaccine coverage is the primary factor influencing the reduction in total cases. The other two parameters, while less significant, become increasingly noticeable as the vaccine coverage increases.

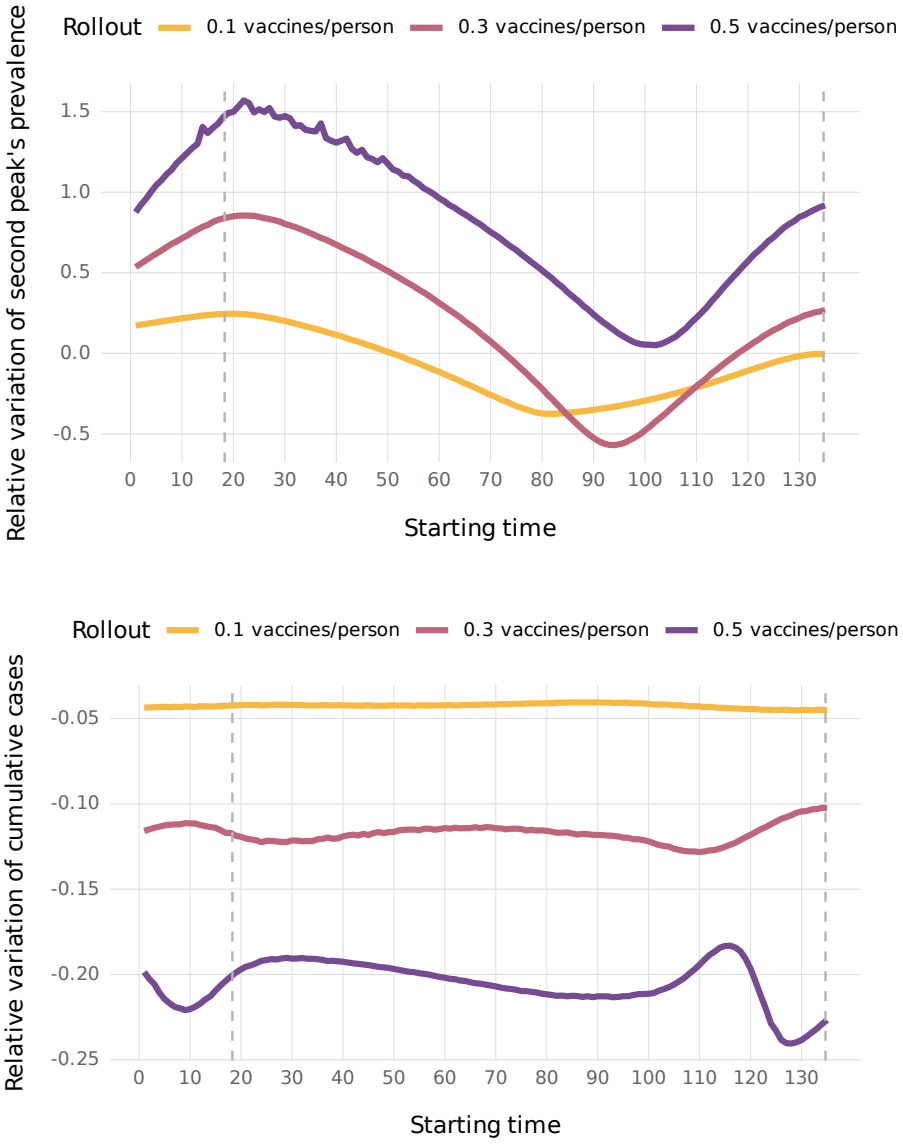

Fig. S3: **Relative variation of the number of cases at the second peak and cumulative cases due to vaccination strategies with varying durations.** The three vaccination volume levels depicted in this figure correspond to 0.1, 0.3 and 0.5 vaccines per person. The duration of each vaccination campaign is constant and equal to 60 days. The curves have been obtained running the SIRS model with vaccination. The horizontal axis is the starting day of the vaccination campaign, and the vertical axis is the relative height variation of the second peak of cases (top), and the cumulative number of cases (bottom). The variation is measured relative to the baseline scenario with no vaccines. The dashed vertical lines indicate the location of the first and second peaks in the baseline simulation. Observing the bottom plot, we see that those strategies that deliver more vaccines over time produce better results in terms of containing the number of cumulative cases. However, looking at the top plot, we see that the same longer duration strategies also cause a larger rebound effect. Simulations run with $\beta = 1$, $\mu = 0.5$, $\delta = 0.01$, $I(0) = 10^{-4}$.

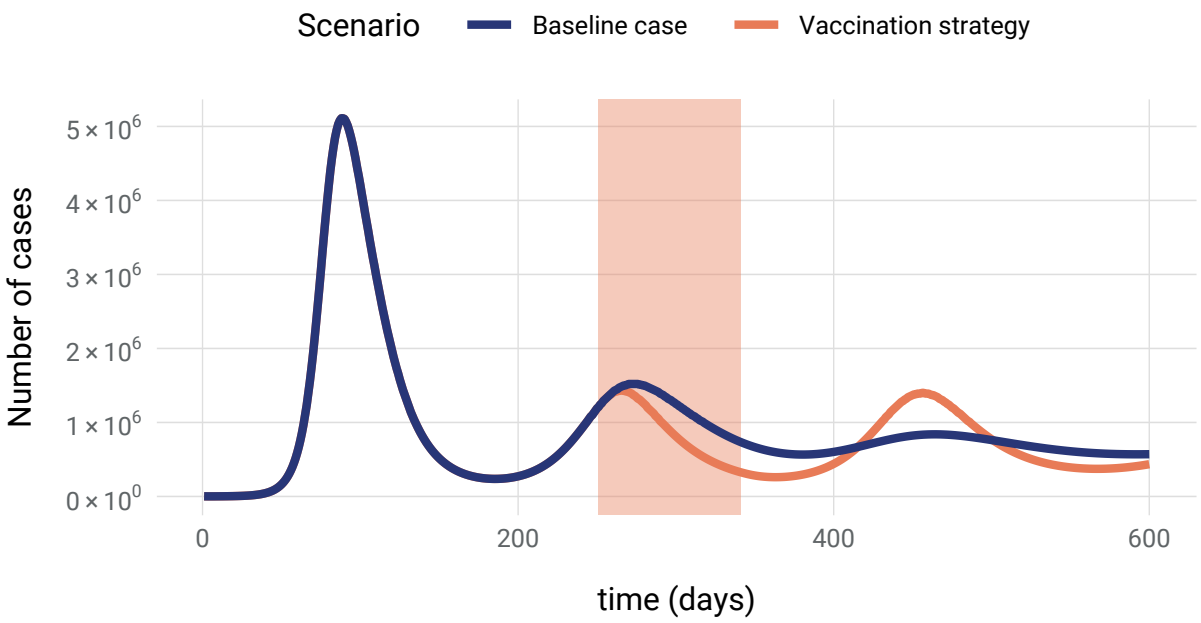

Fig. S4: **Appearance of subsequent peaks due to improper timing of the vaccination strategies.** The dark blue line shows the outcome of the baseline scenario where no vaccination campaign is active, while the orange line is the result of a certain vaccination strategy where the timing of the campaign during the second wave exacerbates the third wave. The shaded area denotes the duration of the campaign, which starts at $t = 251$ and lasts for 90 days. Here, the age priority vector is set to $[0.1, 0.4, 0.5]$. This example shows that an improperly timed vaccination during the second peak can significantly amplify the following third peak. This observation highlights the generalizability of the conclusions regarding the first and second peaks to any consecutive peaks in the epidemic, emphasizing the importance of well-timed vaccination strategies to mitigate the severity of future waves.

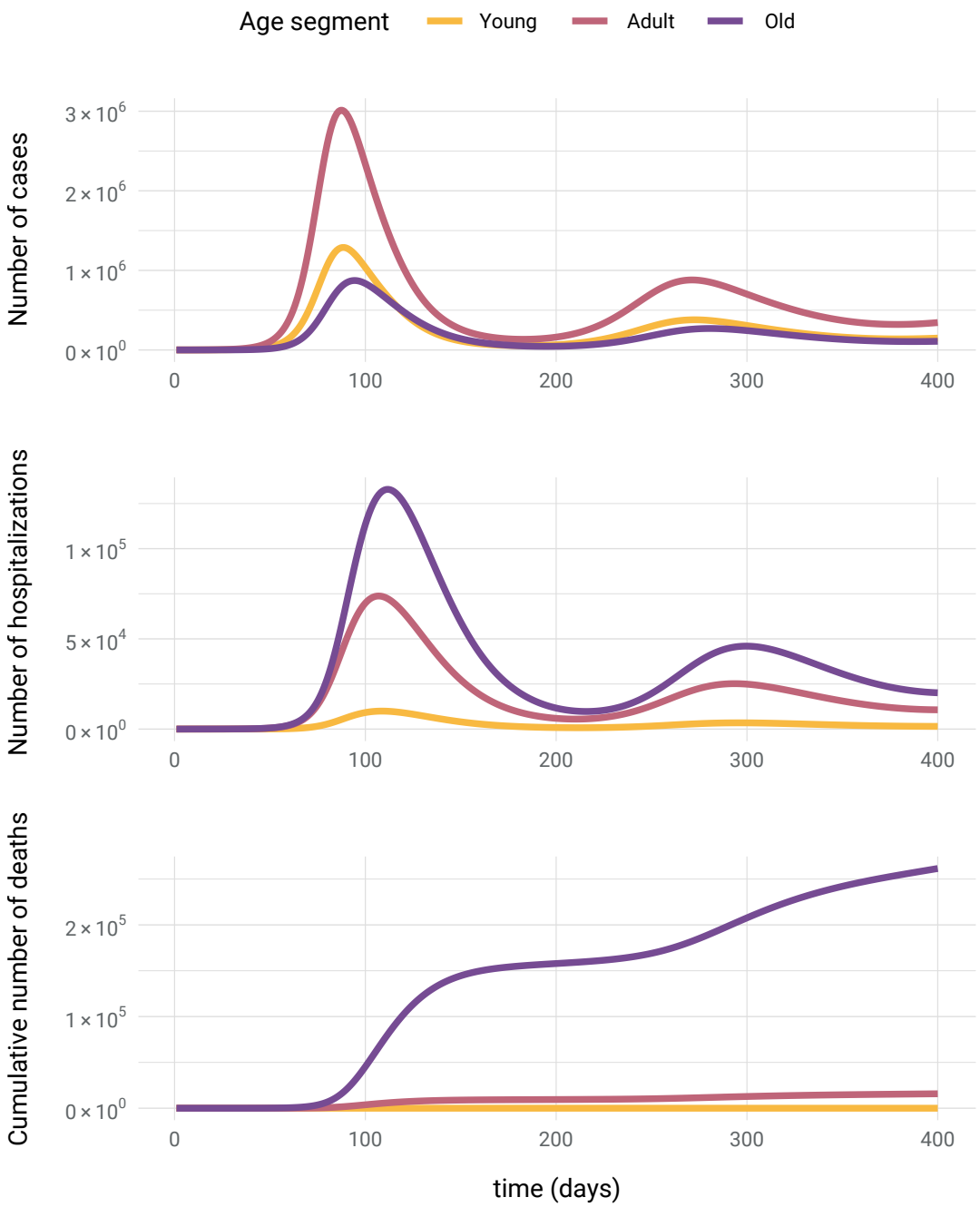

Fig. S5: **Number of cases, hospitalizations and cumulative number of deaths in the baseline scenario, for different age strata.** This figure illustrates the breakdown of cases, hospitalizations, and cumulative deaths in the baseline scenario (without an active vaccination campaign) across different age groups. As we can see on the top plot, the adult population contributes most to active cases, followed by the young and elderly. However, hospitalizations (middle plot) predominantly affect the elderly, followed by adults and the young. In terms of fatalities (bottom plot), the elderly group significantly dominates the numbers.

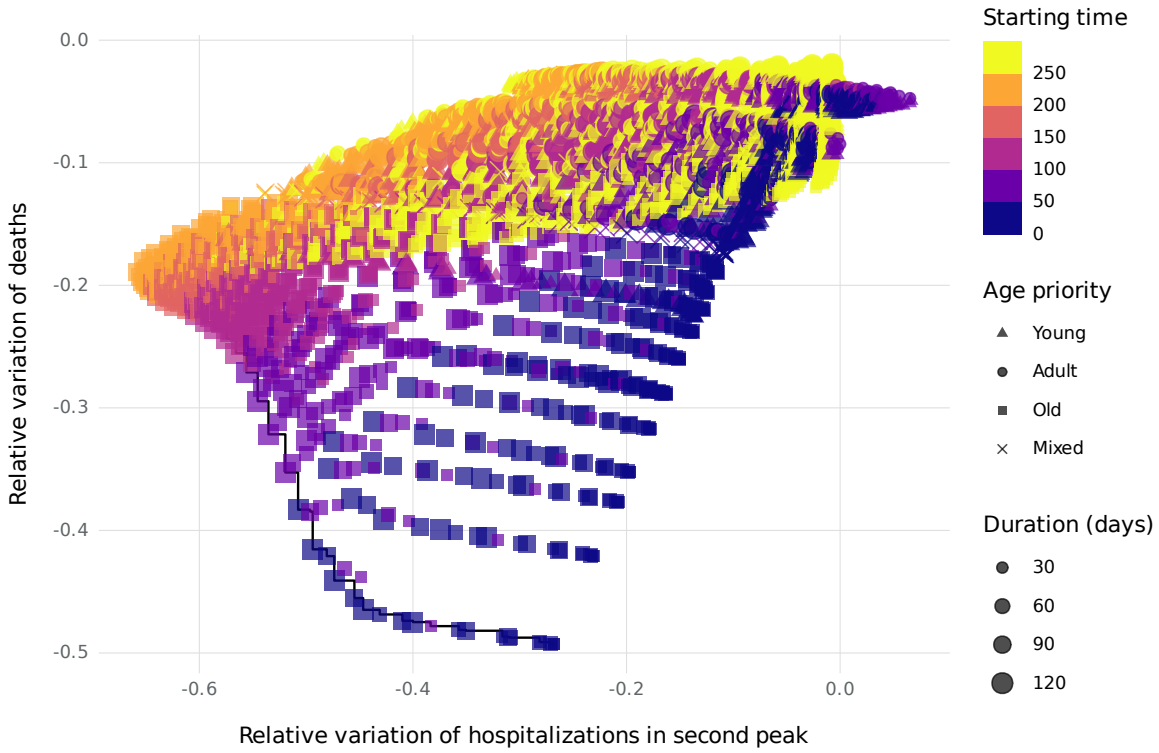

Fig. S6: **Analysis of the vaccination strategies (hospitalizations).** In this scatter plot, each point corresponds to a unique simulation based on a distinct vaccination strategy. The horizontal axis represents the variation in the number of hospitalizations at the second peak relative to the baseline case, whereas the vertical axis depicts the relative variation in the number of deaths. The color, shape, and size of each point carry the same meaning as those in Fig. 6, i.e., they indicate the starting day, age priority, and duration of each vaccination strategy, respectively. The black solid line represents the Pareto front, indicating the optimal strategies that provide the best way to simultaneously minimize hospitalizations and deaths. We can see that in this case, the rebound effect disappears almost completely since in this model vaccines offer long-term protection against hospitalization. The shape of the Pareto front also changes, as the distinction between Type 1 and Type 2 strategies disappears.

Features of the Pareto-optimal strategies

Simulation	Duration	Starting time	Priority vector	
	90	230	[0.1 , 0.2 , 0.7]	O
	90	230	[0.2 , 0.1 , 0.7]	O
*	90	230	[0.1 , 0.1 , 0.8]	O
	120	219	[0.1 , 0.1 , 0.8]	O
*	90	219	[0.1 , 0.1 , 0.8]	O
*	120	207	[0.1 , 0.1 , 0.8]	O
	120	196	[0.2 , 0.1 , 0.7]	O
*	120	196	[0.1 , 0.1 , 0.8]	O
*	120	184	[0.1 , 0.1 , 0.8]	O
	120	173	[0.1 , 0.1 , 0.8]	O
	120	161	[0.1 , 0.1 , 0.8]	O
	120	150	[0.1 , 0.1 , 0.8]	O
	120	138	[0.1 , 0.1 , 0.8]	O
	120	127	[0.1 , 0.1 , 0.8]	O
	120	115	[0.1 , 0.1 , 0.8]	O
	120	104	[0.1 , 0.1 , 0.8]	O
	120	93	[0.1 , 0.1 , 0.8]	O
	120	81	[0.1 , 0.1 , 0.8]	O
	120	70	[0.1 , 0.1 , 0.8]	O
	120	58	[0.1 , 0.1 , 0.8]	O
	120	47	[0.1 , 0.1 , 0.8]	O
	90	58	[0.1 , 0.1 , 0.8]	O
	120	35	[0.1 , 0.1 , 0.8]	O
	90	47	[0.1 , 0.1 , 0.8]	O
	120	24	[0.1 , 0.1 , 0.8]	O
	90	35	[0.1 , 0.1 , 0.8]	O
	120	12	[0.1 , 0.1 , 0.8]	O
	60	47	[0.1 , 0.1 , 0.8]	O
	90	24	[0.1 , 0.1 , 0.8]	O
	120	1	[0.1 , 0.1 , 0.8]	O
	30	58	[0.1 , 0.1 , 0.8]	O
	60	35	[0.1 , 0.1 , 0.8]	O
	90	12	[0.1 , 0.1 , 0.8]	O
	30	47	[0.1 , 0.1 , 0.8]	O
	90	1	[0.1 , 0.1 , 0.8]	O
	60	24	[0.1 , 0.1 , 0.8]	O
*	30	35	[0.1 , 0.1 , 0.8]	O
	60	12	[0.1 , 0.1 , 0.8]	O
	60	1	[0.1 , 0.1 , 0.8]	O
*	30	24	[0.1 , 0.1 , 0.8]	O
	30	1	[0.1 , 0.1 , 0.8]	O
*	30	12	[0.1 , 0.1 , 0.8]	O

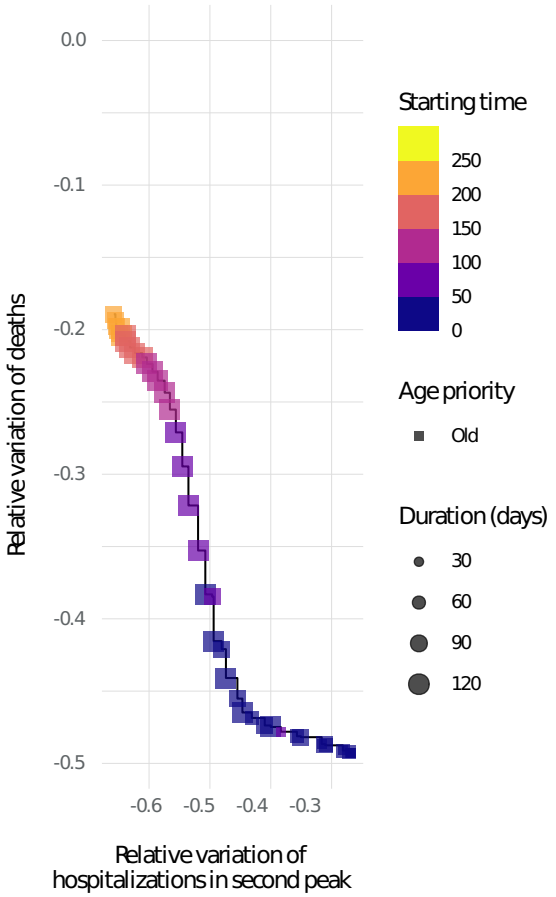

Fig. S7: **Features of the Pareto-optimal strategies (hospitalizations).** This table shows the characteristics of Pareto-optimal strategies alongside a scatter plot that includes only those data points belonging to the Pareto front. The columns of the table provide information on the duration and starting time of each strategy, the priority vector that determines the vaccines distribution by age group (ordered as [Young, Adult, Old]), as well as the age stratum that is most prioritized for each strategy. The asterisk indicates simulations that are optimal for reducing both the number of cases and the number of hospitalizations. As illustrated in the table equivalent to the one presented here, but using cases as the measure (see main text), we can still identify two distinct types of vaccination strategies. However, in this case, the transition between the two kinds is smoother. This can be attributed to the fact that hospitalizations and deaths are more dependent on each other than cases and deaths, and therefore the strategies to optimally reduce one of them are bound to have a certain impact on the other one as well.

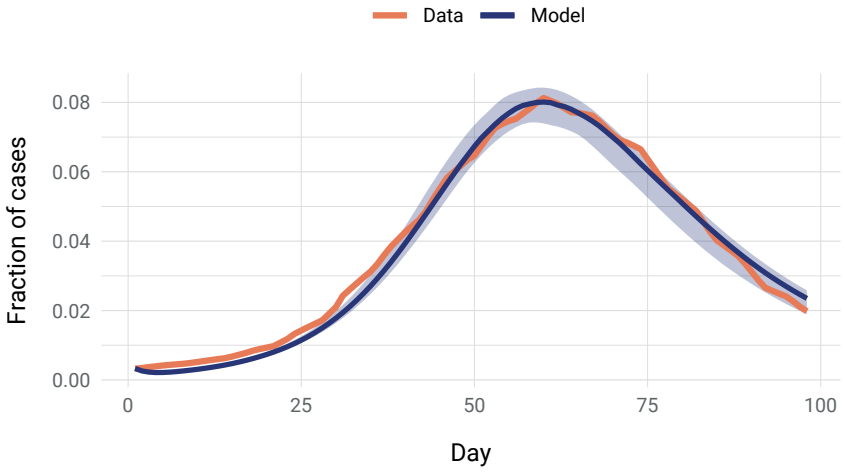

Fig. S8: **Model calibration through the comparison of active cases in Spain.** The time interval considered here goes from the 1st of December 2021 to the 7th of March 2022. The orange line corresponds to real data [1] while the blue line corresponds to the best model prediction. The shadowed area represents the 95% confidence interval.

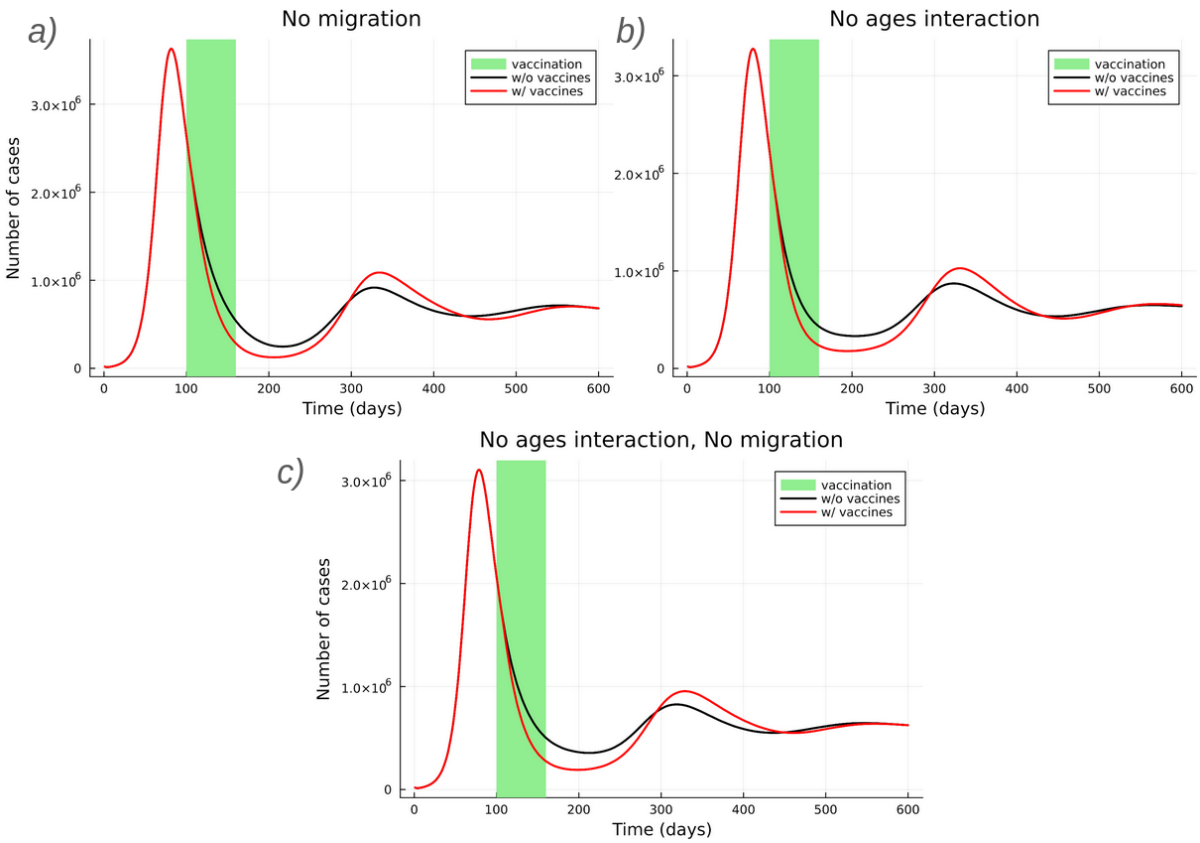

Fig. S9: **Examples of rebound in the absence of ages, migration, or both**. To demonstrate that the rebound effect is independent of both the metapopulation network and the age structure, we present figures where the rebound occurs even when both these factors are excluded. The black lines represent the baseline with no vaccination, while the red lines depict scenarios resulting from vaccination within the time window indicated by the green area. In *a*) and *c*), inter-patch mobility has been disabled by setting all elements of the parameter p^g to zero; in *b*) and *c*) the age structure was eliminated by turning the contact matrix C^{gh} into a diagonal matrix. The rest of the parameters and initial conditions were the same as used in the simulation explained in Sections S3 and S4. It is evident from all three figures that the qualitative behavior is remarkably similar: after a brief period of lower prevalence, the cases in the vaccinated scenarios consistently rise above the baseline in all scenarios, thereby confirming that neither migrations nor age structures are sufficient to disrupt the rebound effect.

Section S1. Rebound timing and its dependence on vaccination

As we already mentioned in the Methods section of the paper, the solution for the infected individuals after the end of an eradication-type vaccination campaign is:

$$I(t) = I(t_{\text{stop}}) \exp\left[(\beta-\mu)(t-t_{\text{stop}}) - \frac{\beta R(t_{\text{stop}})}{\delta}(1-e^{-\delta(t-t_{\text{stop}})})\right]. \tag{S.1}$$

Since it is reasonable to think that the no-infection approximation stops working right around the time the infectious peak is reached, this allows us to use the time t_p where the formula loses meaning as an estimate of the timing of the next epidemic peak. In particular t_p is defined as the time such that $I(t_p) = 1 - \mu/\beta$, which is an upper-bound for the height of any peak. We know this because Eqs. (1)–(3) of the SIRS model imply that, when $\dot{I} = 0$ (e.g., in a maximum for $I(t)$), the value of the susceptible compartment should be $S = \mu/\beta$, which in turn puts a strong constrain on the sum of the other two compartments.

A closed formula for t_p can be obtained using Lambert W function [2] as follows:

$$\begin{aligned} t_p = t_{\text{stop}} &+ \frac{\beta}{\beta-\mu}\frac{R(t_{\text{stop}})}{\delta} - \frac{1}{\beta-\mu}\ln\frac{\beta I(t_{\text{stop}})}{\beta-\mu} \\ &+ \frac{1}{\delta}W\left(-\frac{\beta R(t_{\text{stop}})}{\beta-\mu}\exp\left\{-\frac{\beta R(t_{\text{stop}})}{\beta-\mu} + \frac{\delta}{\beta-\mu}\ln\frac{\beta I(t_{\text{stop}})}{\beta-\mu}\right\}\right). \end{aligned} \tag{S.2}$$

This expression is too complex to be used in regular calculations, but it allows us to understand how the rebound timing t_p depends on the strength of the previous vaccination through its dependencies on $I(t_{\text{stop}})$ and $S(t_{\text{stop}})$. We do this by looking at the partial derivatives $\frac{\partial t_p}{\partial I(t_{\text{stop}})}$ and $\frac{\partial t_p}{\partial S(t_{\text{stop}})}$. We consider $I(t_{\text{stop}})$ and $S(t_{\text{stop}})$ as the independent variables, and substitute $R(t_{\text{stop}})$ using the normalization condition, i.e., $R(t_{\text{stop}}) = 1 - S(t_{\text{stop}}) - I(t_{\text{stop}})$. Thus,

$$\frac{\partial R(t_{\text{stop}})}{\partial I(t_{\text{stop}})} = \frac{\partial R(t_{\text{stop}})}{\partial S(t_{\text{stop}})} = -1\,. \tag{S.3}$$

Furthermore, we will use the following property of the principal branch of the Lambert W function:

$$\frac{\mathrm{d}W(x)}{\mathrm{d}x} = \frac{W(x)}{x(W(x)+1)} > 0\,, \quad \forall x > -\frac{1}{e}\,. \tag{S.4}$$

We introduce two auxiliary variables A and B, where A corresponds to the argument of the exponential inside the Lambert W function, and B is the argument of the Lambert function itself:

$$A = -\frac{\beta R(t_{\text{stop}})}{\beta-\mu} + \frac{\delta}{\beta-\mu}\ln\frac{\beta I(t_{\text{stop}})}{\beta-\mu}\,, \tag{S.5}$$

$$B = -\frac{\beta R(t_{\text{stop}})}{\beta-\mu}\exp\{A\} = -\frac{\beta R(t_{\text{stop}})}{\beta-\mu}\exp\left\{-\frac{\beta R(t_{\text{stop}})}{\beta-\mu} + \frac{\delta}{\beta-\mu}\ln\frac{\beta I(t_{\text{stop}})}{\beta-\mu}\right\}, \tag{S.6}$$

thus Eq. (S.2) can be rewritten as

$$t_p = t_{\text{stop}} - \frac{A}{\delta} + \frac{W(B)}{\delta}\,. \tag{S.7}$$

Before we proceed to calculate the derivatives of the time t_p with respect to $I(t_{\rm stop})$ and $S(t_{\rm stop})$, it is useful to calculate the derivatives of A and B:

$$\frac{\partial A}{\partial I(t_{\rm stop})} = \frac{\beta}{\beta-\mu} + \frac{\delta}{I(t_{\rm stop})(\beta-\mu)}\,, \tag{S.8}$$

$$\frac{\partial A}{\partial S(t_{\rm stop})} = \frac{\beta}{\beta-\mu}\,, \tag{S.9}$$

$$\frac{\partial B}{\partial I(t_{\rm stop})} = B\left(\frac{\partial A}{\partial I(t_{\rm stop})} - \frac{1}{R(t_{\rm stop})}\right), \tag{S.10}$$

$$\frac{\partial B}{\partial S(t_{\rm stop})} = B\left(\frac{\partial A}{\partial S(t_{\rm stop})} - \frac{1}{R(t_{\rm stop})}\right). \tag{S.11}$$

Note that Eqs. (S.8) and (S.9) are always positive. Armed with these definitions we write the first partial derivative of t_p as follows:

$$\frac{\partial t_p}{\partial I(t_{\rm stop})} = -\frac{1}{\delta}\frac{\partial A}{\partial I(t_{\rm stop})} + \frac{1}{\delta}\frac{{\rm d}W(B)}{{\rm d}B}\frac{\partial B}{\partial I(t_{\rm stop})} \tag{S.12}$$

$$= -\frac{1}{\delta}\frac{\partial A}{\partial I(t_{\rm stop})} + \frac{1}{\delta}\frac{{\rm d}W(B)}{{\rm d}B}B\left(\frac{\partial A}{\partial I(t_{\rm stop})} - \frac{1}{R(t_{\rm stop})}\right) \tag{S.13}$$

$$= -\frac{1}{\delta}\frac{\partial A}{\partial I(t_{\rm stop})} - \frac{1}{\delta}\frac{{\rm d}W(B)}{{\rm d}B}\frac{\beta R(t_{\rm stop})}{\beta-\mu}\exp\{A\}\left(\frac{\partial A}{\partial I(t_{\rm stop})} - \frac{1}{R(t_{\rm stop})}\right). \tag{S.14}$$

We immediately notice that this partial derivative is negative if the term in the parenthesis is positive, which can be written as

$$\frac{\partial A}{\partial I(t_{\rm stop})} - \frac{1}{R(t_{\rm stop})} > 0 \quad\Longleftrightarrow\quad R(t_{\rm stop}) > \frac{(\beta-\mu)I(t_{\rm stop})}{\beta I(t_{\rm stop})+\delta}\,. \tag{S.15}$$

Since we are currently working with vaccination, in the eradication regime we can safely assume that $I(t_{\rm stop}) \ll 1$ and, therefore, that the above inequality is satisfied and

$$\frac{\partial t_p}{\partial I(t_{\rm stop})} < 0\,. \tag{S.16}$$

On the other hand, the other partial derivative reads

$$\frac{\partial t_p}{\partial S(t_{\rm stop})} = -\frac{1}{\delta}\frac{\partial A}{\partial S(t_{\rm stop})} + \frac{1}{\delta}\frac{{\rm d}W(B)}{{\rm d}B}\frac{\partial B}{\partial S(t_{\rm stop})} \tag{S.17}$$

$$= -\frac{1}{\delta}\frac{\partial A}{\partial S(t_{\rm stop})} + \frac{1}{\delta}\frac{{\rm d}W(B)}{{\rm d}B}B\left(\frac{\partial A}{\partial S(t_{\rm stop})} - \frac{1}{R(t_{\rm stop})}\right) \tag{S.18}$$

$$= -\frac{1}{\delta}\frac{\beta}{\beta-\mu} - \frac{1}{\delta}\frac{{\rm d}W(B)}{{\rm d}B}\frac{\beta R(t_{\rm stop})}{\beta-\mu}\exp\{A\}\left(\frac{\beta}{\beta-\mu} - \frac{1}{R(t_{\rm stop})}\right). \tag{S.19}$$

As before, this expression is negative if the term inside the parenthesis is positive. We can write such condition as

$$\frac{\beta}{\beta-\mu} - \frac{1}{R(t_{\rm stop})} > 0 \quad\Longleftrightarrow\quad S(t_{\rm stop}) < \frac{\mu}{\beta}\,, \tag{S.20}$$

which is always true in the eradication regime, therefore proving that, in this scenario,

$$\frac{\partial t_p}{\partial S(t_{\rm stop})} < 0\,. \tag{S.21}$$

To sum up, what we have found is that, the smaller $I(t_{\rm stop})$ and $S(t_{\rm stop})$, the larger t_p will be. Furthermore, since in the eradication regime both of these quantities are related to the rate of vaccination α, what we have demonstrated here is that, the stronger the vaccination campaign (i.e., the larger α), the more delayed the rebound will be.

Section S2. Rebound height and its dependence on vaccination

Finding a good way of estimating the height of an epidemic peak is challenging, and every estimate ends up relying on a number of uncontrolled assumptions. However, in our case we are not so much interested in its numerical estimation, but in finding a formula that displays a similar qualitative behavior.

Our estimate of the epidemic peak relies on the connection between it and the slope of the susceptible curve at time t_p. The two are connected by the Eq. (1) in the following way:

$$\dot{S}(t_p) = -\beta S(t_p) I(t_p) + \delta R(t_p)\,. \tag{S.22}$$

By using the facts that $S(t_p) = \mu/\beta$ and $R(t) = 1 - S(t) - I(t)$, rearranging the terms we get that:

$$I(t_p) = I^* - \frac{\dot{S}(t_p)}{\mu + \delta}\,, \tag{S.23}$$

where $I^* = \frac{\delta}{\mu+\delta}\left(1 - \frac{\mu}{\beta}\right)$ is the equilibrium value of the epidemic compartment in the SIRS model without vaccination. Notice that Eq. (S.23) holds true for every maximum and minimum of the function $I(t)$, but we are here only interested in the first maximum.

The problem now becomes to find the slope of the function $S(t)$ at time t_p. We achieve this with a quadratic approximation $\hat{S}(t) = at^2 + bt + c$ that satisfies the following three conditions:

$$\hat{S}(t_{\max}) = S_{\max}, \qquad \hat{S}(t_p) = \frac{\mu}{\beta}, \qquad \hat{S}'(t_{\max}) = 0, \tag{S.24}$$

where $S_{\max}$ is the maximum value reached by the susceptible compartment before it starts to decrease, while $t_{\max}$ is the time at which that happens. In our approximation we make this point coincide with the vertex of the parabola. The three conditions in Eq. (S.24) give us a system of three equations with three unknowns, i.e., the parameters of the parabola. It is therefore always possible to find an explicit solution:

$$a = -\frac{S_{\max} - \mu/\beta}{(t_p - t_{\max})^2}, \qquad b = -2t_{\max}a, \qquad c = S_{\max} + at_{\max}^2\,. \tag{S.25}$$

Next, we can simply compute the derivative of the parabola at time t_p, $\hat{S}(t_p) = 2at_p + b$, which gives us an estimate for the slope of the susceptible curve at that point

$$\dot{S}(t_p) = -2\frac{S_{\max} - \mu/\beta}{t_p - t_{\max}}\,. \tag{S.26}$$

Finally, thanks to Eq. (S.23), we get an estimate for the height of the peak as a function of the peak in susceptibles preceding the rebound

$$I(t_p) = I^* + \frac{2(S_{\max} - \mu/\beta)}{(\mu + \delta)(t_p - t_{\max})}\,. \tag{S.27}$$

The conclusion we can draw from this estimation is that, the larger the build-up in susceptibles before an epidemic wave (i.e., $S_{\max}$), the taller the subsequent peak will be.

Section S3. Equations of the age-stratified COVID-19 model

The variables of our system of equations are $\{\rho_{i,v}^{m,g}(t)\}$, which indicate the density of individuals in the compartment m, age stratus g, location i and vaccination status v at time t (measured in days). In the following, we write the equations for the temporal evolution of these quantities. Note that, for the majority of these compartments, the indexes g, i and v can be left implicit, while in the case of the compartment S, the index v must be specified because the form of the equation changes according to it. Apart from adding the vaccination state, only the equations for compartments S and R have been changed with respect to the work by Arenas et al. [3]:

$$\rho_{i,0}^{S,g}(t+1) = (1-\Pi_{i,0}^{g}(t))\rho_{i,0}^{S,g}(t) - \epsilon_i^g/n_i^g\,, \tag{S.28}$$

$$\rho_{i,1}^{S,g}(t+1) = (1-\Pi_{i,1}^{g}(t))\rho_{i,1}^{S,g}(t) - \Lambda\rho_{i,1}^{S,g}(t) + \epsilon_i^g(t)/n_i^g\,, \tag{S.29}$$

$$\rho_{i,2}^{S,g}(t+1) = (1-\Pi_{i,2}^{g}(t))\rho_{i,2}^{S,g}(t) + \Lambda\rho_{i,1}^{S,g}(t) + \Gamma(\rho_{i,0}^{R,g}(t) + \rho_{i,1}^{R,g}(t) + \rho_{i,2}^{R,g}(t))\,, \tag{S.30}$$

$$\rho_{i,v}^{E,g}(t+1) = (1-\eta^g)\rho_{i,v}^{E,g}(t) + \Pi_{i,v}^{g}(t)\rho_{i,v}^{S,g}(t)\,, \tag{S.31}$$

$$\rho_{i,v}^{A,g}(t+1) = (1-\alpha^g)\,\rho_{i,v}^{A,g}(t) + \eta^g\,\rho_{i,v}^{E,g}(t)\,, \tag{S.32}$$

$$\rho_{i,v}^{I,g}(t+1) = (1-\mu^g)\,\rho_{i,v}^{I,g}(t) + \alpha^g\,\rho_{i,v}^{A,g}(t)\,, \tag{S.33}$$

$$\rho_{i,v}^{P_D,g}(t+1) = (1-\zeta^g)\,\rho_{i,v}^{P_D,g}(t) + \mu^g\,\theta_v^g\,\rho_{i,v}^{I,g}(t)\,, \tag{S.34}$$

$$\rho_{i,v}^{P_H,g}(t+1) = (1-\lambda^g)\,\rho_{i,v}^{P_H,g}(t) + \mu^g\,(1-\theta_v^g)\,\gamma_v^g\,\rho_{i,v}^{I,g}(t)\,, \tag{S.35}$$

$$\rho_{i,v}^{H_D,g}(t+1) = (1-\psi^g)\,\rho_{i,v}^{H_D,g}(t) + \lambda^g\,\omega_v^g\,\rho_{i,v}^{P_H,g}(t)\,, \tag{S.36}$$

$$\rho_{i,v}^{H_R,g}(t+1) = (1-\chi^g)\,\rho_{i,v}^{H_R,g}(t) + \lambda^g\,(1-\omega_v^g)\,\rho_{i,v}^{P_H,g}(t)\,, \tag{S.37}$$

$$\rho_{i,v}^{D,g}(t+1) = \rho_{i,v}^{D,g}(t) + \zeta^g\,\rho_{i,v}^{P_D,g}(t) + \psi^g\,\rho_{i,v}^{H_D,g}(t)\,, \tag{S.38}$$

$$\rho_{i,v}^{R,g}(t+1) = \rho_{i,v}^{R,g}(t) + \mu^g\,(1-\theta_v^g)\,(1-\gamma_v^g)\,\rho_{i,v}^{I,g}(t) + \chi^g\,\rho_{i,v}^{H_R,g}(t) - \Gamma\rho_{i,v}^{R,g}(t)\,. \tag{S.39}$$

The following normalization relations hold:

$$\sum_{m}\sum_{v\in\{0,1,2\}}\rho_{i,v}^{m,g}(t) = 1, \quad \forall g,i,t, \tag{S.40}$$

which can be easily checked by looking at the system of Eqs. (S.28) to (S.39).

Let us describe the compartmental dynamics of our model. The three vaccination statuses, denoted by $0,1,2$, represent the natural progression of vaccine-associated defense changes within an individual. Respectively, they correspond to: a completely defenseless person; a person with high defenses against both infection and hospitalization; and finally, a person with high defenses against hospitalization but who remains totally susceptible to infection. Initially, a fraction ϵ_i^g/n_i^g of the susceptible population is vaccinated. Although vaccinated individuals will still go through the same epidemiological compartments, their transition rates will differ based on their vaccination status. We assume that vaccine-induced immunity diminishes with rate Λ. Susceptible individuals become infected when they come into contact with asymptomatic or infected individuals, with the probability of transmission denoted by $\Pi_{i,v}^g$ (further explained in the next section). If transmission occurs, the previously susceptible individual moves to the exposed compartment. An exposed individual transitions to the asymptomatic compartment with rate η^g and subsequently to the infected compartment with rate α^g. From the infected compartment, several outcomes are possible, that are reached at a rate μ_v^g. One possibility is recovering after the infection without hospitalization, with probability $(1-\theta_v^g)\,(1-\gamma_v^g)$. Another possibility is having a severe course of infection and requiring hospitalization, with probability $(1-\theta_1^g)\gamma_1^g$ and a delay governed by rate λ^g. At this point, individuals can either receive a

fatal prognosis with probability ω_v^g leading to death at a rate ψ^g, or a good prognosis with probability $1-\omega_v^g$, leading to recovery at a rate χ^g. The last possibility is dying without being hospitalized with probability θ_v^g after a latency period governed by rate ζ^g. Finally, individuals in the recovered compartment who are not vaccinated might transition again to the susceptible compartment with probability Γ. All the numerical values of these parameters can be found in Tables **S1**, **S2** and **S3**.

Section S4. Social contacts and infection probability

It is important to specify how the infection probability $\Pi_{i,v}^g(t)$ is calculated. This probability represents the probability of an individual associated to patch i, age stratum g, and vaccination status v to be infected at time t. Following Arenas et al. [3], the infection probability is calculated as

$$\Pi_{i,v}^g(t) = (1-p^g)P_{i,v}^g(t) + p^g \sum_j R_{ij}^g P_{j,v}^g(t)\,, \tag{S.41}$$

where the first term indicates the probability of susceptible individuals to get infected in their "home" patch while the second term indicates the probability of getting infected elsewhere. In particular p^g is the probability to travel from your patch to another and R_{ji}^g is the probability that an individual of age g will go from i to j, given that it will move (no correlation is assumed between the vaccination status v and the mobility of an individual). Furthermore $P_{i,v}^g(t)$ denotes the probability that an agent of age g and status v gets infected inside patch i. This is, in turn, expressed as

$$P_{i,v}^g(t) \;=\; 1 - \prod_{h,j,w} \prod_{m\in\{A,I\}} \Big[1-\beta^m(1-r_v)(1-b_w)\Big]^{T_{j\to i}^{m,h,w}}\,, \tag{S.42}$$

where r_v is the vaccine efficacy in preventing infections while b_w is the vaccine efficacy in preventing transmission once already infected. The exponent $T_{j\to i}^{m,h,w}$ indicates the effective number of contacts made by an agent of age h, compartment m (either infected of asymptomatic) and vaccination status w that traveled from patch j to patch i. This quantity is calculated as follows:

$$T_{j\to i}^{m,h,v} = z^g \langle k^g\rangle f(n_i^g/s_i) C^{gh} \frac{n_{j\to i}^{m,h,v}}{\tilde{n}_i^h}\,. \tag{S.43}$$

Here, the term $z^g \langle k^g\rangle f(n_i^g/s_i)$ represents the total number of contacts that people of age g make inside patch i. Those contacts increase monotonically with the population density in that patch, and the function that we use to model this dependency is the following [3]:

$$f(x) = 1 + (1-e^{-\xi x})\,. \tag{S.44}$$

Since we want the overall number of contacts to depend on the average number of connections of each age group, we introduce $\langle k^g\rangle$ multiplied by a normalization factor z^g such that the average degree of population belonging to age group g is exactly $\langle k^g\rangle$. From [3] we know that:

$$z^g = \frac{n^g}{\sum_{i=1}^{N_P} f(\frac{\tilde{n}_i}{s_i})\tilde{n}_i^g}\,, \tag{S.45}$$

where s_i is the surface of the patch i, and the symbols $\tilde{n}_i$ and $\tilde{n}_i^g$ refer to the number of people present in patch i during the commuting phase, given by:

$$\tilde{n}_i = \sum_{g=1}^{N_G} \tilde{n}_i^g \tag{S.46}$$

and

$$\tilde{n}_i^g = \sum_{j=1}^{N_P} M_{ji}^g n_j^g \,, \tag{S.47}$$

For convenience, we also define the mobility matrix as

$$M_{ji}^g = (1 - p^g)\delta_{ji} + p^g R_{ji}^g \,, \tag{S.48}$$

being δ_{ji} the Kronecker delta function. Then, the total number of contacts must be multiplied by C^{gh}, which specifies the fraction of all the contacts that individuals in age group g have with individuals in age group h. Finally, the last term in the exponent indicates how many of these contacts were with infected or asymptomatic people coming from node j:

$$n_{j\to i}^{m,h,v}(t) = n_j^h \rho_{j,v}^{m,h}(t) M_{ji}^h \,. \tag{S.49}$$

All the numerical values of the parameters in this section can be found in Table **S4**.

Symbol	Description	Estimates in Spain	Assignment
β^I	Infectivity of symptomatic	0.056	Calibrated
β^A	Infectivity of asymptomatic	$\beta^I/2$	Assumed
η^g	Exposed rate	0.127	Calibrated
α^g	Asymptomatic rate	0.306	Calibrated
μ^g	Infectious rate	0.589	Calibrated

Table S1: **Epidemic parameters.** Parameters of the epidemic, determined through calibration with real data on the number of active cases of COVID-19 in Spain between the 1st of December 2021 and the 7th of March 2022 [1], see Fig. **S8**. The calibration was carried out using the Turing package of the Julia language, which relies on a Markov Chain Monte Carlo approach with a No-U-Turn sample [4].

Symbol	Description	Estimates in Spain	Assignment
θ_v^g	Direct death probability	0.0	[5]
$\{\gamma_v^g\}$	ICU probability	$(0.003, 0.01, 0.08)^g \otimes (0, 0.15)_v$	[5, 6]
$\{\omega_v^g\}$	Death probability in ICU	$(0, 0.04, 0.3)^g \otimes (0, 0.1)_v$	[5, 6]
λ^g	Prehospitalized in ICU rate	4.084 days^{-1}	[3]
ζ^g	Predeceased rate	7.084 days^{-1}	[3]
ψ^g	Death rate in ICU	7 days^{-1}	[3]
χ^g	ICU discharge rate	21 days^{-1}	[3]

Table S2: **Clinical parameters.** Clinical parameters, taken from Arenas et al. [3].

Symbol	Description	Estimates in Spain	Assignment
Γ	Reinfection rate	100 days^{-1}	Assumed
Λ	Waning immunity rate	50 days^{-1}	Assumed
$\{r_v\}$	Risk Reduction of infection probability	$(0.0, 0.6)$	[6]
$\{b_v\}$	Risk Reduction of transmission probability	$(0.0, 0.4)$	[6]

Table S3: **Vaccination and immunity parameters.** Selected vaccination and immunity parameters.

Symbol	Description	Estimates for $g \in \{Y, M, O\}$ in Spain
$\{N^g\}$	Population by age stratum	(12M, 26,4M, 8,9M) [7]
n_i^g	Region population	[8]
s_i	Region surface	[8]
R_{ij}^g	Mobility matrix (non-diagonal)	[9]
$\langle k^g \rangle$	Average total number of contacts	[3]
C^{gh}	Contacts-by-age matrix	[3]
ξ	Density factor	0.01 km^2 [3]
$\{p^g\}$	Mobility factor	$(0.3, 1.0, 0.05)$ [3]

Table S4: **Social parameters.** Parameters of the model related to geographic and population data, including mobility, and their values for Spain.

References

[1] Worldmeter. Active cases in spain, 2022.

[2] Rob M. Corless, Gaston H. Gonnet, David E. G. Hare, David J. Jeffrey, and Donald E. Knuth. On the Lambert W function. *Advances in Computational Mathematics*, 5(1):329–359, 1996.

[3] Alex Arenas, Wesley Cota, Jesús Gómez-Gardeñes, Sergio Gómez, Clara Granell, Joan T. Matamalas, David Soriano-Paños, and Benjamin Steinegger. Modeling the spatiotemporal epidemic spreading of COVID-19 and the impact of mobility and social distancing interventions. *Physical Review X*, 10:041055, 2020.

[4] Matthew D Hoffman, Andrew Gelman, et al. The No-U-Turn sampler: adaptively setting path lengths in Hamiltonian Monte Carlo. *Journal of Machine Learning Research*, 15(1):1593–1623, 2014.

[5] Informe n.120. Situación de COVID-19 en España. Technical report, Red Nacional de Vigilancia Epidemiológica, 2022.

[6] COVID-19 Vaccine surveillance report. Report, UK Health Security Agency, 2022.

[7] Instituto Nacional de Estadística. Resident population by date, sex and age, 2021.

[8] Instituto Geografico Nacional. Datos geográficos y toponimia, 2011.

[9] Mobilidad y Agenda Urbana Ministerio de Transportes. Estudio de movilidad con big data durante la pandemia. Technical report.